Phase diagram, structure, and electronic properties of $(Ga_{1-x}Zn_{x})(N_{1-x}O_{x})$ solid solutions from DFT-based simulations

Li Li, James T. Muckerman, Mark S. Hybertsen, and Philip B. Allen

Phys. Rev. B **83**, 134202 — Published 11 April 2011

DOI: 10.1103/PhysRevB.83.134202

Phase diagram, structure and electronic properties of $(Ga_{1-x}Zn_x)(N_{1-x}O_x)$ solid solution from DFT-based simulations

Li Li,[1,*] James T. Muckerman,[2] Mark S. Hybertsen,[3] and Philip B. Allen[1,†]

[1] *Department of Physics and Astronomy, Stony Brook University, Stony Brook, NY 11794-3800*
[2] *Chemistry Department, Brookhaven National Laboratory, Upton, NY 11973*
[3] *Center for Functional Nanomaterials, Brookhaven National Laboratory, Upton, NY 11973*

We construct an accurate cluster expansion (CE) for the $(Ga_{1-x}Zn_x)(N_{1-x}O_x)$ solid solution, based on density functional theory (DFT). The subsequent Monte Carlo simulation reveals a phase diagram, which has a wide miscibility gap and an x=0.5 ordered compound. The disordered phase displays strong short range order (SRO) at synthesis temperatures. To study the influences of SRO on the lattice and electronic properties, we conduct DFT calculations on snapshots from the MC simulation. Consistent with previous theoretical and experimental findings, lattice parameters were found to deviate from Vegard's law with small upward bowing. Bond lengths depend strongly on local environment, with a variation much larger than the difference of bond length between ZnO and GaN. The downward band gap bowing deviates from parabolic by having a more rapid onset of bowing at low and high concentrations. An overall bowing parameter of 3.3 eV is predicted from a quadratic fit to the compositional dependence of the calculated band gap. Our results indicate that SRO has significant influence over both structural and electronic properties.

PACS numbers: 61.66.Dk, 64.75.Nx, 71.20.Nr

I. INTRODUCTION

The $(Ga_{1-x}Zn_x)(N_{1-x}O_x)$ solid solution is a visible-light-driven photocatalyst for water splitting.[1,2] Band gap reduction is crucial for improving solar photon absorption efficiency. Diffuse reflectance spectroscopy measurements indicate a band gap bowing parameter of 3∼4 eV.[3,4] The band gap of the 50% alloy is around 2.4 eV,[4] much more efficient for solar applications than either GaN and ZnO, with E_g equal to 3.4 and 3.2 eV, respectively.

Theory addresses the electronic structure from various approaches.[5–9] As pointed out by Wang et al. (Ref. 9), strong short range order appears in the alloy. A correct model must take this ordering into account. In the present paper, we use the cluster expansion (CE) formalism[10–14] to construct a model Hamiltonian from density functional theory (DFT). Thermodynamic properties are calculated through Monte Carlo simulation. The effect of ordering on structural and electronic properties is examined based on DFT calculations for a sample of supercells extracted from snapshots from the MC calculation.

II. MODEL AND METHOD

We model the solid solution as a wurtzite lattice with equal composition of Ga and N, and no atom exchange between cation and anion sublattices, similar to the approach adopted in our previous work.[7] Thus the formula is $(Ga_{1-x}Zn_x)(N_{1-x}O_x)$. These assumptions are consistent with experimental results.[4,15,16] In first principles calculations, we assume the atoms reside on this lattice with bond lengths and bond angles allowed to relax. Recent diffraction data for a sample near $x = 1/8$ was best fit with a split-site anion model indicative of significant deviations from a uniform wurtzite structure.[17] In this study, we restrict the lattice sites for the anions to those from the wurtzite structure, although this assumption may need to be revisited when more complete experimental information becomes available. Point defects such as vacancies, interstitials and cation/anion substitutions are also beyond the scope of this paper. Our goal is to understand the atom site occupancy of the crystalline alloy at thermal equilibrium as a function of temperature, and its influence on the lattice parameters, bonds, and band gaps.

The CE[10–14] is a standard tool in thermodynamic studies of alloys. Once constructed, it only requires the site occupancy as input to predict the formation energy E of a specific configuration, where E is defined as

$$E = E_{\text{alloy}} - xE_{\text{ZnO}} - (1-x)E_{\text{GaN}}. \tag{1}$$

Positional relaxation is implicitly included in our CE parameters but does not appear explicitly. This method uses an Ising-like model with spins σ_i on site i to represent occupation. If site i is a cation site, then $\sigma = 1$ denotes Zn and $\sigma = -1$ denotes Ga. Similarly, if site i is an anion site, then $\sigma = 1$ denotes O and $\sigma = -1$ denotes N. The total energy per 4-atom primitive cell is the sum of the relevant one, two, and many body interactions.

$$E = \sum_{\alpha} m_\alpha J_\alpha \langle \prod_{i \in \alpha'} \sigma_i \rangle \tag{2}$$

The index α is used to enumerate symmetry-inequivalent clusters, with multiplicity m_α per primitive unit cell. The bracket gives the average spin product for all clusters which are symmetrically equivalent to each other. The effective cluster interactions (ECI) J_α are obtained by fitting to a database of DFT energies of fully relaxed

structures. The initial database contains randomly generated structures. It gives an initial CE model, which is then used to generate new trial structures in the low and medium energy range, in an attempt to explore the site occupancy space efficiently. This method has been successfully applied to a wide range of systems including metals, semiconductors, oxides, etc. It has also been generalized to treat multisublattice systems.[18] The $(Ga_{1-x}Zn_x)(N_{1-x}O_x)$ solid solution is a two-sublattice example, which contains not only clusters belonging to a single (cation or anion) sublattice, but also clusters containing both (see Fig. 1). The two-sublattice cluster expansion, if all clusters are taken into account, gives a complete basis set for the site occupancy space. The error of the cluster expansion construction is measured by the "leave-many-out" cross validation score (LMO-CV)[19–23]. Following the procedure described in Ref. 23, we split the database into construction data sets and validation data sets. The validation data set contains 30 percent of the entire database. For a specific selection of clusters, we fit the CE parameters using the construction data set, then calculate the mean squared error of prediction (MSEP) for the validation data set. The final LMO-CV is estimated by averaging the MSEP over $2N$ random splits of the input database of size N. To select appropriate clusters, a range of basis set cutoffs is examined to minimize the prediction error.[24] Routines in the ATAT package[25–30] are used to do the cluster expansion construction and the subsequent Monte Carlo simulation.

Monte Carlo simulation is used to investigate the thermodynamic properties and phase diagram. The simulation uses a $14 \times 14 \times 8$ supercell with periodic boundary conditions. We only allow MC moves that change the number of Ga and N by the same amount, so that the stoichiometric constraint is satisfied. The equilibration of the structure and averaging of thermodynamic quantities takes at least 50,000 steps/atom. Convergence tests suggest that the accuracy of the energy averaging is better than 0.2 meV/atom.

First principles calculations use the VASP package.[31] We choose the PBE[32] implementation for the exchange-correlation functional and the PAW[33,34] basis set for the expansion of wave functions. The plane wave cutoff is 500 eV. An $8 \times 8 \times 6$ k-point mesh is used for the wurtzite GaN and ZnO primitive cell. For supercells, the k-point meshes are adjusted to have as similar density to the primitive cell k-mesh as possible. All self-consistent calculations are converged to 0.1 meV. For structural relaxation, a conjugate gradient algorithm reduces the force on each atom to less than 0.05 eV/Å. Gallium and zinc 3d electrons are treated explicitly as valence electrons.

DFT underestimates the band gap for GaN and ZnO and overestimates the 3d band energies. To partially prevent the alloy from incorrectly becoming metallic in the DFT calculation, we apply an on-site Coulomb interaction U[35,36] to the 3d orbitals of gallium and zinc. The values of U (from Ref. 7) are 3.9 eV and 6.0 eV, respectively. These values were shown[7] to be the best to reproduce lattice parameters and band gaps. After the correction, the 3d band positions and the band gaps of GaN and ZnO (2.4 eV and 1.6 eV, respectively) lie closer to the experimental values.

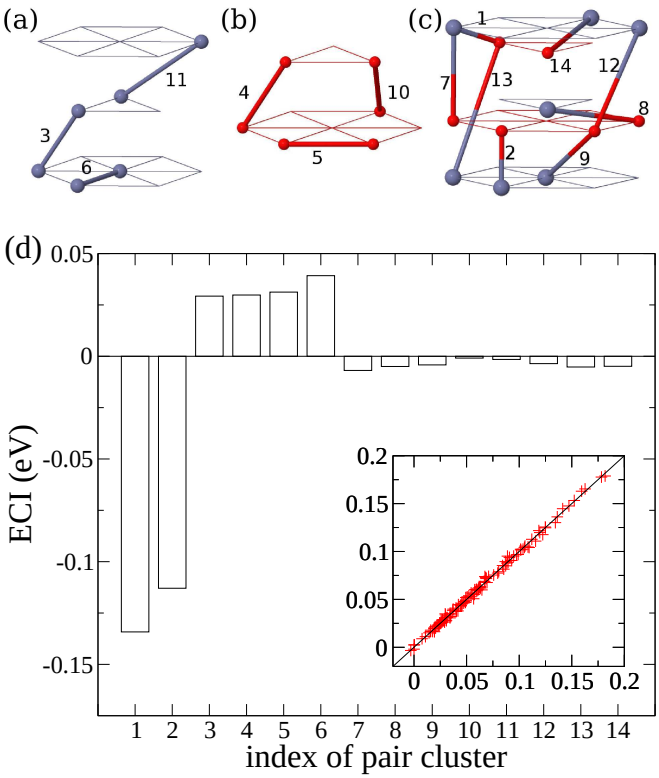

FIG. 1. (color online). Numbering of clusters and calculated effective cluster interactions (ECI). Zero and one-body clusters are not shown in the figure. The ECI's are indexed by the separation of their constituent atoms. The distance of pair 14 is 5Å. (a) Cation-cation clusters. (b) Anion-anion clusters. (c) Cation-anion clusters. (d) Effective cluster interactions. Inset: comparison of formation energy between CE prediction (y-axis) and DFT calculation (x-axis), in units of eV/atom.

III. RESULTS AND DISCUSSIONS

A. Cluster Expansion Construction

Figure 1 and Table I show the selected clusters and calculated effective cluster interactions for all the relevant clusters in the present paper. We construct the cluster expansion using a database of 120 structures calculated by DFT (up to a $4 \times 4 \times 3$ supercell). The CE contains 1 zero-body cluster, 2 one-body clusters (cation site and anion site), and 14 pair clusters. The ECI for the two one-body clusters are degenerate due to the constraint of equal number of Ga and N atoms. This selection of clusters gives the minimum "leave-many-out" cross validation score of 3 meV/atom. Our tests show that including longer-range pair clusters or many-body clusters does

TABLE I. Values of ECI in meV. The indexing of the two-body clusters is shown in Fig. 1. The zero-body term is normalized to one primitive cell.

zero-body	one-body		two-body				
	cation	anion	1	2	3	4	5
495.69	-2.20	-2.20	-134.19	-112.95	29.29	29.82	31.24

two-body								
6	7	8	9	10	11	12	13	14
39.25	-6.89	-4.96	-4.19	-0.88	-1.55	-3.59	-5.24	-4.88

not further reduce the LMO-CV. Like a well-behaved CE construction, the magnitude of the effective cluster interactions J_α decreases as the separation between the constituent atoms increases. Nearest neighbor interactions (clusters 1,2 in Fig.1) give the dominant contributions to the formation energy. The negative sign indicates a strong *clustering* tendency, e.g., Ga prefers N neighbors rather than O neighbors. This is due to the matching valence charge in Ga-N and Zn-O bonds rather than Ga-O and Zn-N bonds in a tetrahedrally-coordinated environment. The difference between the ECI of pair 1 and pair 2 shows that the *clustering* tendency in the *ab*-plane is stronger than along the *c*-axis. All of the second neighbor interactions are positive, indicating an *ordering* tendency, which represents a repulsion between the same species, e.g., Ga prefers Zn as a second neighbor rather than Ga. These two competing tendencies determine the short range order we will discuss later.

B. Monte Carlo simulation

Monte Carlo simulations are performed to investigate the equilibrium thermodynamic properties. Figure 2(a) shows the formation energy averaged over thermal ensembles of configurations as a function of temperature. At $x = 0.5$, the alloy is predicted to undergo a first-order phase transition from an ordered compound to the disordered phase as T increases above 870 K. At $x = 0.25$, the disordered phase is predicted to exist above 760 K, and to become phase separated at lower temperature. Actual samples have not been found with these long-range orders, presumably because 870 K is too low for equilibration to occur.

Based on the MC simulation, we propose a theoretical phase diagram (Fig. 3) for the $(Ga_{1-x}Zn_x)(N_{1-x}O_x)$ solid solution. It has a wide miscibility gap and an $x = 0.5$ stable compound. The stable compound has layered ordering in the (0001) direction as shown in (Fig. 3(b)), with the same periodicity as the wurtzite structure. The atoms are arranged so that, among the four first neighbors of Ga, there are three N atoms and one O; among the twelve second neighbors of Ga, there are six Zn and six Ga atoms. Zn, N and O atoms experience a similar environment. This structure is a delicate compromise between the *clustering* tendency for first neighbor and the *ordering* tendency for second neighbor. Its formation energy is about −3 meV/atom, barely stabilized against phase separation into GaN and ZnO.

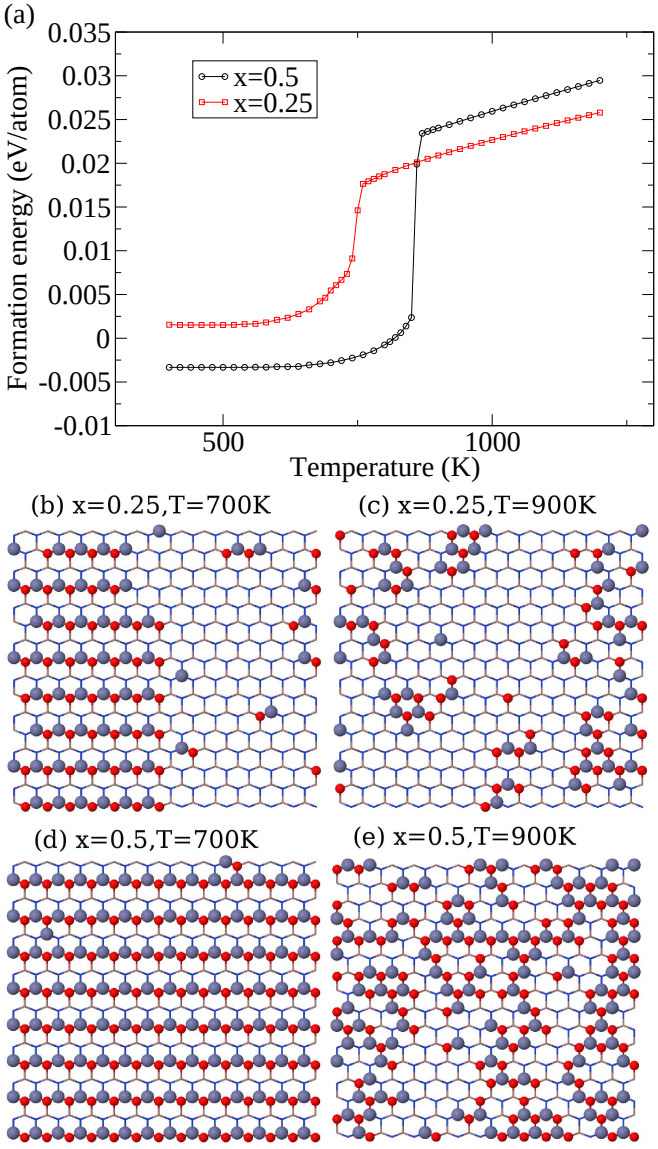

FIG. 2. (color online). (a) Formation energies of the solid solution $(Ga_{1-x}Zn_x)(N_{1-x}O_x)$ calculated from Monte Carlo simulation at concentrations $x = 0.5$ and $x = 0.25$. (b)(c)(d)(e) Snapshots from the Monte Carlo simulation. Only a $14 \times 1 \times 8$ slice of the $14 \times 14 \times 8$ simulation cell is shown. In the graph, the horizontal direction is the wurtzite a lattice vector. The vertical direction is the c vector. Small (red) balls: Oxygen; Large (blue) balls: Zinc; Gallium and Nitrogen atoms are hidden.

In our simulations, the disordered phase displays strong short range *clustering* (Fig. 2(c) and (e)). This effect can be quantified by the Warren-Cowley short range

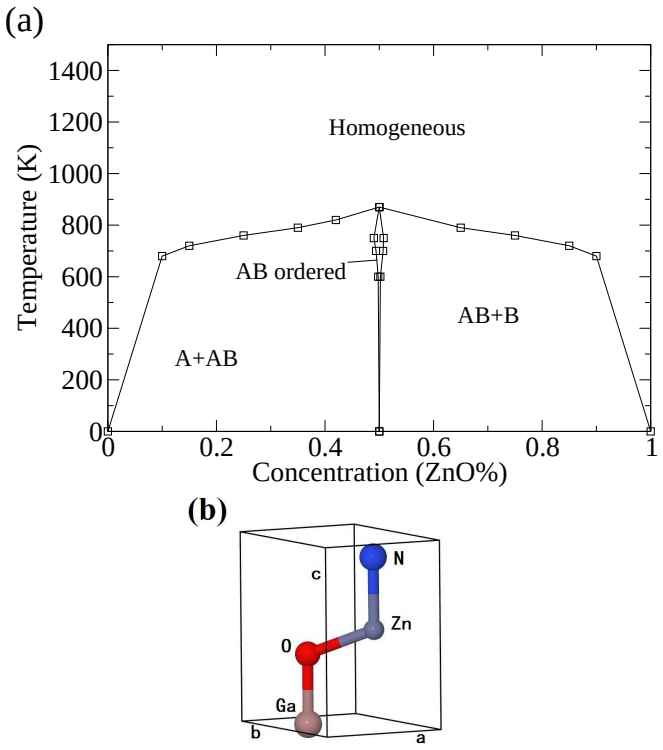

FIG. 3. (color online). (a) Computed phase diagram of $(Ga_{1-x}Zn_x)(N_{1-x}O_x)$ solid solution. Straight lines are guides to the eye. Phase A is mostly GaN. Phase B is mostly ZnO. Phase AB is the ordered superlattice structure. (b) Ball-stick model of the ordered AB compound.

order (SRO) parameter α_{lmn}, defined as

$$\alpha_{lmn}(x,T) = 1 - \frac{P_{lmn}^{A(B)}(x,T)}{x}, \qquad (3)$$

where x is the concentration of ZnO, T is the equilibration temperature, $P_{lmn}^{A(B)}$ is the conditional probability of finding a B atom in the lmn shell, given that the center atom is A. There are three types of SRO in the $(Ga_{1-x}Zn_x)(N_{1-x}O_x)$ solid solution. For a pair of cation sites, A is Ga and B is Zn. For a pair of anion sites, A is N and B is O. For a pair of cation and anion sites, A is Ga and B is O. Positive SRO indicates *clustering* and negative indicates *ordering*. Figure 4 shows the calculated SRO at $x = 0.2$ and $T = 1200$ K. The SRO is positive for first and second neighbor shells; it quickly decays to zero at and beyond the third neighbor. This *clustering* tendency persists to very high temperatures (see inset in Fig.4). Therefore, the SRO is an inherent characteristic of the $(Ga_{1-x}Zn_x)(N_{1-x}O_x)$ solid solution. It remains relatively constant within the range of synthesis temperatures and can not be removed.

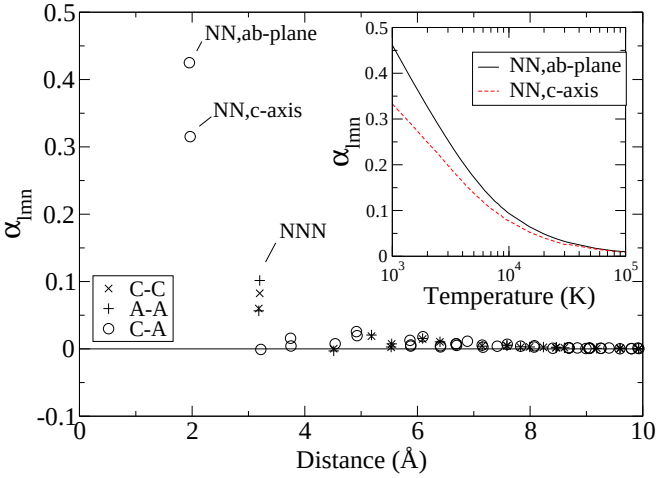

FIG. 4. Calculated SRO for x=0.2 and T=1200 K. Each point represents a different type of pair (C-C: cation-cation pair; A-A: anion-anion pair; C-A: cation-anion pair; NN: nearest neighbor; NNN: next nearest neighbor). Inset: temperature dependence of SRO for the first neighbors in ab-plane and c-axis.

C. Lattice Parameters, Bond Lengths and Band Gaps

The Monte Carlo simulation based on the cluster expansion can only predict site occupancies. It can not provide direct information about coordinate relaxation or electronic structure. However, we can obtain this information from DFT. The investigation of lattice parameters, bond lengths and band gaps contains two steps. First, we conduct Monte Carlo simulation and equilibrate the structure at a specific temperature and concentration. Then, we randomly draw snapshots from the simulation and use them to do DFT calculations. Due to DFT's limited capability of handling large structures, we restrict the supercell to be $4 \times 4 \times 3$, with 192 atoms. To average over the fluctuations due to the finite size of the simulation cell, four snapshots are taken at each temperature and concentration. We estimate the quantities of interest, e.g., band gap, from DFT calculations of these snapshots.

Actual $(Ga_{1-x}Zn_x)(N_{1-x}O_x)$ samples at room temperature do not show the ordered binary or phase-separated structures, because low atom mobility below 900 K inhibits equilibration. Since the temperature dependence of SRO is relatively weak (see fig. 4), we adopt 1200 K as a reasonable effective equilibration temperature characterizing actual samples at lower temperature. Although the measurements of band gaps, etc., are conducted at room temperature, it is appropriate to compare with theory at the higher effective equilibration temperature.

Figure 5 shows the lattice parameters extracted from DFT calculations of these snapshots. As comparisons, we also considered snapshots from a MC temperature of 5000 K, which exhibits half as much SRO (see inset

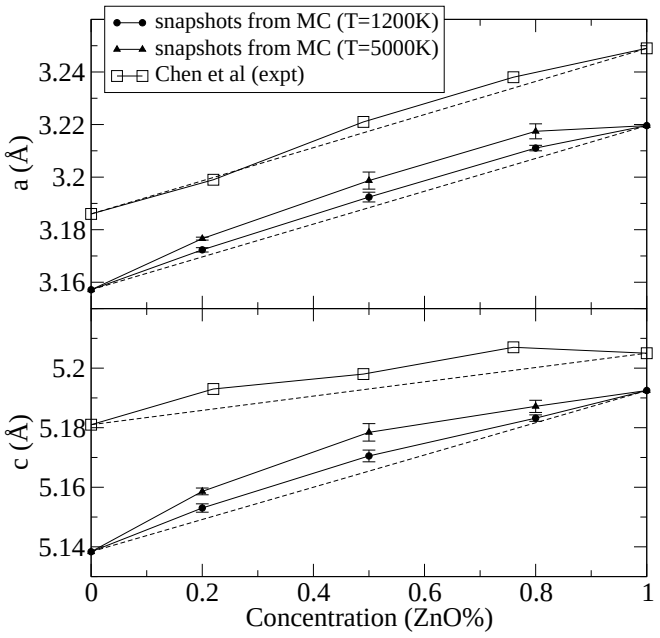

FIG. 5. Filled symbols show the lattice parameters from DFT based on MC snapshots. The error bars cover twice the standard deviation of underlying snapshots (four per point). Open symbols show the experimental results (Ref. 4). Dashed lines show the predictions from Vegard's law.

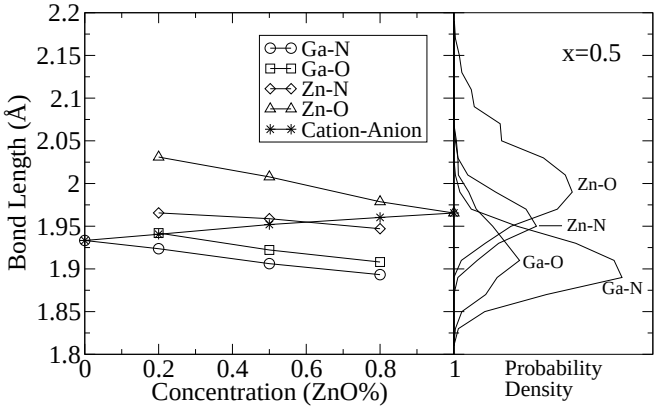

FIG. 6. (Left) Average bond lengths of snapshots from T=1200 K MC simulation. (Right) Probability distribution of bond types and bond lengths at x=0.5

of Fig.4). In reality, the sample would decompose at such a high temperature; we use it here simply to study the influence of ordering. We find the upward bowing predicted from snapshots at 5000 K to be approximately twice that found at 1200 K. Greater disorder causes the lattice parameters to increase. Experimentally, c bows more than a,[4] whereas DFT gives equal bowing. The overall agreement on the magnitude of upward bowing suggests that SRO exists in the samples reported by Chen et al.[4]

Figure 6 shows the analysis of cation-anion (nearest neighbor) bond lengths. Although the bond in the ZnO

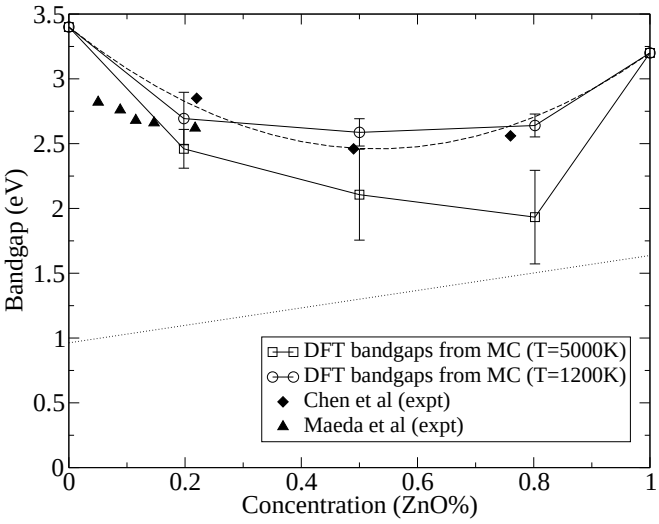

FIG. 7. Comparison of band gaps between DFT and experiment. Open symbols represent DFT results on snapshots described in previous figures. DFT results have been shifted up by the dotted line (Eq. (5)) to enable comparison with experimental data. The dashed line is the parabolic fitting of the DFT results, with a bowing parameter of 3.34 eV. Diamonds are the experimental values from Chen et al. (Ref. 4). Triangles are the experimental results from Maeda et al. (Ref. 3).

crystal is longer than that in GaN, the difference becomes even larger in the alloy. The Ga-N bond shrinks further and the Zn-O bond expands upon mixing. This unusual bond relaxation is a consequence of the non-isovalent nature of the alloy. ZnSe-GaAs system shows the similar behavior,[37] in which the Zn-Se bond expands and the Ga-As bond shrinks. However, the average bond length for all cation-anion bonds follows approximately a linear relationship. This is due to the change in the proportion of different types of bond, i.e., there are more Zn-O bonds in a ZnO-rich condition.

Figure 7 shows the comparison between calculated and measured band gaps. To correct for the well-known errors in the band gap as calculated with DFT, a composition-dependent adjustment is included. For any structure σ with composition $x(\sigma)$, the adjusted band gap is

$$E_{g,\mathrm{adjusted}}(\sigma) = E_{g,\mathrm{DFT}}(\sigma) + \Delta(x), \qquad (4)$$

where

$$\begin{aligned}\Delta(x) =&(1-x)(E_{g,\mathrm{expt}}(\mathrm{GaN}) - E_{g,\mathrm{DFT}}(\mathrm{GaN})) \\ &+ x(E_{g,\mathrm{expt}}(\mathrm{ZnO}) - E_{g,\mathrm{DFT}}(\mathrm{ZnO})). \qquad (5)\end{aligned}$$

A useful quantity in the analysis of alloy band gaps is the bowing parameter b, defined as

$$E_g(\sigma) = (1-x)E_g(\mathrm{GaN}) + xE_g(\mathrm{ZnO}) - bx(1-x), \quad (6)$$

which, for any configuration σ, describes its deviation (in parabolic approximation) from linear interpolation between the two end points. The band gap from snapshots of 1200 K MC simulation is symmetric but not

perfectly parabolic. The bowing is slightly greater at low and high ZnO concentrations. Compared to 1200 K, the snapshots from 5000 K MC simulation have much larger bowing parameters, indicating a red shift of band gap, induced by disorder, consistent with Wang et al.[9] The asymmetric behavior is due to the different band gap reducing mechanism at the dilute limit.[6] Using Eq. (6), the fitted bowing parameter at 1200 K is 3.34 eV. Our previous work, which does not take the strong short range order into account, predicted the bowing parameter to be 4.05 eV.[7] Compared to experiments, the band gap of 1200 K MC snapshots closely follows the value from the high temperature and high pressure synthesised samples (Chen et al.[4]). It also agrees well with the 22% ZnO sample from Maeda et al.[3] In the regime of lower ZnO concentration, the trend of our calculated data requires a bowing parameter greater than 3.34 eV. Indeed, the theoretical investigation by Wang et al.[9] predicted the bowing parameter for the 12.5% alloy to be 4.8 eV (at 1100 K). The experimental results from Maeda et al.[3] indicates the bowing parameter increases with decreasing ZnO concentration, from ∼4 eV at 22%, to ∼12 eV at 5%. In summary, we find that both concentration and disorder causes band gap bowing to deviate from a simple T-independent parabola.

IV. CONCLUSION

We present a cluster expansion model for $(Ga_{1-x}Zn_x)(N_{1-x}O_x)$ solid solutions which accurately extrapolates DFT energies. Monte Carlo simulation reveals a phase diagram with a wide miscibility gap and an $x = 0.5$ stable compound below 870 K. At synthesis temperatures, the solid solution is in the disordered phase. Strong short range order is an inherent property and remains relatively constant within the likely range of equilibration temperatures. Based on snapshots from MC simulation, we investigate the structure and electronic properties by DFT. The lattice parameters are found to deviate from Vegard's law. The upward bowing is increased by randomness. The relaxation of bond lengths is unusual and can be attributed to the different valences of GaN and ZnO. Short range order also induces a blue shift in the band gap.

ACKNOWLEDGMENTS

We are grateful for discussions with members of SWaSSiT group including Maria V. Fernandez-Serra, Yolanda A. Small, Wei Kang, Xiao Shen and Jue Wang. This research used computational resources: (i) at the New York Center for Computational Sciences at Stony Brook University/Brookhaven National Laboratory which is supported by the U.S. Department of Energy under Contract No. DE-AC02-98CH10886 and by the State of New York; (ii) at the Center for Functional Nanomaterials, Brookhaven National Laboratory, which is supported by the U.S. Department of Energy under Contract No. DE-AC02-98CH10886; and (iii) of the Seawulf cluster at the Stony Brook University. Work at Stony Brook was supported initially by AERTC and subsequently by DOE grant DE-FG02-08ER46550. The work at BNL was supported by the US DOE under contract DE-AC02-98CH10886 (by its Division of Chemical Sciences and its Scientific User Facilities Division).

* lili4@ic.sunysb.edu
† philip.allen@sunysb.edu

[1] K. Maeda, T. Takata, M. Hara, N. Saito, Y. Inoue, H. Kobayashi, and K. Domen, J. Am. Chem. Soc. **127**, 8286 (2005).
[2] K. Maeda, K. Teramura, D. Lu, T. Takata, N. Saito, Y. Inoue, and K. Domen, Nature **440**, 295 (2006).
[3] K. Maeda, K. Teramura, T. Takata, M. Hara, N. Saito, K. Toda, Y. Inoue, H. Kobayashi, and K. Domen, J. Phys. Chem. B **109**, 20504 (2005).
[4] H. Chen, L. Wang, J. Bai, J. C. Hanson, J. B. Warren, J. T. Muckerman, E. Fujita, and J. A. Rodriguez, J. Phys. Chem. C **114**, 1809 (2010).
[5] W. Wei, Y. Dai, K. Yang, M. Guo, and B. Huang, J. Phys. Chem. C **112**, 15915 (2008).
[6] M. N. Huda, Y. Yan, S.-H. Wei, and M. M. Al-Jassim, Phys. Rev. B **78**, 195204 (2008).
[7] L. L. Jensen, J. T. Muckerman, and M. D. Newton, J. Phys. Chem. C **112**, 3439 (2008).
[8] C. Di Valentin, J. Phys. Chem. C **114**, 7054 (2010).
[9] S. Wang and L.-W. Wang, Phys. Rev. Lett. **104**, 065501 (2010).
[10] D. D. Fontaine, Solid State Phys. **47**, 33 (1994).
[11] J. W. D. Connolly and A. R. Williams, Phys. Rev. B **27**, 5169 (1983).
[12] J. M. Sanchez, F. Ducastelle, and D. Gratias, Physica A **128**, 334 (1984).
[13] F. Ducastelle, *Order and Phase Stability in Alloys* (Elsevier Science, New York, 1991).
[14] A. Zunger, in *First principles statistical mechanics of semiconductor alloys and intermetallic compounds*, NATO Advanced Studies Institute, Series B: Physics (Plenum, New York, 1994).
[15] M. Yashima, K. Maeda, K. Teramura, T. Takata, and K. Domen, Chem. Phys. Lett. **416**, 225 (2005).
[16] H. Chen, W. Wen, Q. Wang, J. C. Hanson, J. T. Muckerman, E. Fujita, A. I. Frenkel, and J. A. Rodriguez, J. Phys. Chem. C **113**, 3650 (2009).
[17] M. Yashima, H. Yamada, K. Maeda, and K. Domen, Chem. Commun. **46**, 2379 (2010).
[18] P. D. Tepesch, G. D. Garbulsky, and G. Ceder, Phys. Rev. Lett. **74**, 2272 (1995).
[19] S. Geisser, J. Amer. Statistical Assoc. **70**, 320 (1975).
[20] M. Stone, J. R. Stat. Soc., B **39**, 44 (1977).

[21] J. Shao, J. Amer. Statistical Assoc. **88**, pp. 486 (1993).
[22] P. Zhang, Ann. Statist. **21**, 299 (1993).
[23] K. Baumann, TrAC, Trends Anal. Chem. **22**, 395 (2003).
[24] N. A. Zarkevich and D. D. Johnson, Phys. Rev. Lett. **92**, 255702 (2004).
[25] A. van de Walle, M. Asta, and G. Ceder, Calphad **26**, 539 (2002).
[26] A. van de Walle and M. Asta, Modelling and Simulation in Materials Science and Engineering **10**, 521 (2002).
[27] A. van de Walle and G. Ceder, J. Phase Equilib. **23**, 348 (2002).
[28] A. van de Walle, Calphad **33**, 266 (2009).
[29] G. L. W. Hart and R. W. Forcade, Phys. Rev. B **77**, 224115 (2008).
[30] D. B. Laks, L. G. Ferreira, S. Froyen, and A. Zunger, Phys. Rev. B **46**, 12587 (1992).
[31] G. Kresse and J. Furthmüller, Phys. Rev. B **54**, 11169 (1996).
[32] J. P. Perdew, K. Burke, and M. Ernzerhof, Phys. Rev. Lett. **77**, 3865 (1996).
[33] P. E. Blöchl, Phys. Rev. B **50**, 17953 (1994).
[34] G. Kresse and D. Joubert, Phys. Rev. B **59**, 1758 (1999).
[35] A. I. Liechtenstein, V. I. Anisimov, and J. Zaanen, Phys. Rev. B **52**, R5467 (1995).
[36] S. L. Dudarev, G. A. Botton, S. Y. Savrasov, C. J. Humphreys, and A. P. Sutton, Phys. Rev. B **57**, 1505 (1998).
[37] L. G. Wang and A. Zunger, Phys. Rev. B **68**, 125211 (2003).